

# Session 2P7

## Electromagnetic Theory and Dielectric Waveguides and Antennas

<p>Theory of Rain Fades; Measurement Done at Ku-band Satellite Link in a Tropical Region  <i>V. Kumar (University of the South Pacific, Fiji); V. Ramachandran (University of the South Pacific, Fiji);</i> .....</p> <p>The Characteristics of Millimetre-wave Gyrotropic Magnetic Material for Use in Quasi-optical Non-reciprocal Devices  <i>B. Yang (Queen Mary, University of London, UK); R. S. Donnan (Queen Mary, University of London, UK); D. H. Martin (Queen Mary, University of London, UK);</i> .....</p> <p>“Wiggly-line” Perturbation Applying to Ground Plane Aperture for Multispurious Rejection in Microstrip Parallel Coupled Line Filter  <i>M. Moradian (Isfahan University of Technology, Iran); M. R. Hajhashemi (Isfahan University of Technology, Iran); S. V. Mirmoghtadaie (Isfahan University, Iran);</i> .....</p> <p>Design of a Non-uniform High Impedance Surface for a Low Profile Antenna  <i>M. Hosseini (Iran Telecommunication Research Center (ITRC), Iran); A. Pirhadi (Tarbiat Modares University, Iran); M. Hakkak (Tarbiat Modares University, Iran);</i> .....</p> <p>Axial Focusing Properties of Cosine-Gaussian Beam by a Lens with Spherical Aberration  <i>Q. F. Wang (Southwest Jiaotong University, China); X. Q. Wang (Southwest Jiaotong University, China); L. Wang (Southwest Jiaotong University, China); J. J. Lin (Southwest Jiaotong University, China); J. S. Tang (Southwest Jiaotong University, China); K. Sheng (Southwest Jiaotong University, China);</i> ....</p> <p>Some Applications of the High-mode-merging Method  <i>J. Tang (Southwest Jiaotong University, China); X. Wang (Southwest Jiaotong University, China); L. Wang (Southwest Jiaotong University, China); S. Cao (Southwest Jiaotong University, China); Z. Wang (NC A and T State University, USA); J. Gao (Southwest Jiaotong University, China); K. Sheng (Southwest Jiaotong University, China);</i> .....</p> <p>Analysis of Circular Cavity with Metalized Dielectric Posts or Corrugated Cylinders  <i>R. Lech (Gdansk University of Technology, Poland); J. Mazur (Gdansk University of Technology, Poland);</i></p> <p>UWB Textile Antennas for Wearable Applications  <i>M. Klemm (Swiss Federal Institute of Technology, Switzerland); G. Troester (Swiss Federal Institute of Technology, Switzerland);</i> .....</p> <p>Propagation of Strong Electromagnetic Waves in Semiconductors with S-shaped Current Voltage Characteristics  <i>Y. G. Gurevich (Universidad de Salamanca, Spain); J. E. Velázquez-Pérez (Universidad de Salamanca, Spain);</i> .....</p> <p>Effect of Surface Defects on the Amplification of Anomalous Transmission in Dielectric and Metallic Photonic Band Gap Materials: Calculation and Experimental Verification  <i>S. Massaoudi (UniversitéPairs-Sud, France); A. Ourir (UniversitéPairs-Sud, France); A. de Lustrac (UniversitéPairs-Sud, France);</i> .....</p> <p>Dielectric Waveguide Filter with Cross Coupling  <i>D. S. Jun (Electronics and Telecommunications Research Institute, Korea); H. Y. Lee (Electronics and Telecommunications Research Institute, Korea); D. Y. Kim (Electronics and Telecommunications Research Institute, Korea); S. S. Lee (Electronics and Telecommunications Research Institute, Korea); E. S. Nam (Electronics and Telecommunications Research Institute, Korea); K. I. Cho (Electronics and Telecommunications Research Institute, Korea);</i> .....</p>	<p>668</p> <p>669</p> <p>670</p> <p>671</p> <p>676</p> <p>677</p> <p>682</p> <p>683</p> <p>684</p> <p>685</p> <p>686</p>
---	--

## Theory of Rain Fades; Measurement Done at Ku-band Satellite Link in a Tropical Region

V. Kumar and V. Ramachandran  
University of the South Pacific, Fiji

The results on rain attenuation measurements made on 11.65 GHz signal from INTELSAT 701 at Suva (Lat.: 18.08° S, Long.: 178.3° E), a tropical region, during the period of Apr'02–Mar'03 are presented in this paper. Rainfall at Suva was often frequent and heavy with average accumulation per month exceeding 150 mm. In the tropics, heavy rainfall has intense pockets of rain surrounded by larger regions of less intense rainfall. Rain-rate and attenuation measurement showed good correlation, since the site had a high elevation angle of 68.5, which increases the probability of having only one rain cell in the propagation path. Deep fades ( $> 7$  dB) on 11.65 GHz were often short lived. They collectively occurred for 7.4 hrs of year at the site and were mostly recorded during the evening hours. Fading occurs through the process of absorption (minor) and scattering (major) by water droplets present in the propagation path. The finite conductivities of the water droplets make it an imperfect dielectric (complex quantity) medium and at 11.65 GHz, attenuation due to absorption is calculated to be 0.015 dB/km. The absorption coefficient ( $\alpha$ ) increases with frequency. The process of attenuation by scattering is determined by the scattering parameter  $\delta$ , which is a function of the radii of the raindrops and the frequency of the signal. At the observed frequency, Rayleigh scattering happens when it is drizzling and in cloud and fog where each molecule in a droplet behaves like an individual dipole which scatters the radiowave in all directions. Mie scattering occurs at high rain-rate where the drop size is comparable or larger than the wavelength, hence, the Fresnel's relation for the reflection and transmission of the EM wave at the boundary of two media (water and air) of different refractive indices are applicable. The imperfection in the dielectric constant leads to a complex transmission coefficient and as a result, causes the received signal to be depolarized.

# The Characteristics of Millimetre-wave Gyrotropic Magnetic Material for Use in Quasi-optical Non-reciprocal Devices

B. Yang, R. S. Donnan, and D. H. Martin  
Queen Mary, University of London, UK

Ferrites materials are employed in many millimetre-wave and sub-millimetre-wave applications such as radar, imaging, communications, electron spin resonance and precision measurement. The use of quasi-optical techniques are preferable for millimetre-wave systems over waveguiding for the propagation and manipulation of signals as they afford low power losses, wide bandwidths and high power handling capabilities.

Large numbers of quasi-optical Faraday rotators utilize magnetically soft ferrite material. These devices are biased by using large external magnets. Quasi-optical Faraday rotators that used permanently magnetized ferrites were first examined by Martin et al. [1] who surveyed a number of ferrites and produced an isolator with 17 dB isolation and 1.0 dB insertion loss at 115 GHz. This work was extended and improved upon by Webb [2] who produced W-band isolators having 30 dB isolation and an insertion loss of  $< 0.5$  dB.

The objective of our research is to focus on selecting magnetically-hard ferrite materials, which are ideally suited to operate in high frequency ( $> 90$  GHz) quasi-optical non-reciprocal devices.

In this paper we present the static magnetic characteristics of a candidate material, which is suited for use in high-performance non-reciprocal device operating at frequency above 90 GHz. Further, we theoretically examine the determination of a ferrite's magneto-optical constants from complex amplitude reflectance and transmittance measurements, and assess the stability of such determinations upon measurement practice.

## REFERENCES

1. Wylde, R. J., "Gaussian beam-mode circuits for millimetre wavelengths," Ph.D. Thesis, Queen Mary University of London, 1985.
2. Webb, M. R., "Millimetre wave quasi-optical signal processing systems," Ph.D. Thesis, St Andrews, 1992.

# “Wiggly-line” Perturbation Applying to Ground Plane Aperture for Multispurious Rejection in Microstrip Parallel Coupled Line Filter

**M. Moradian and M. R. Hajhashemi**  
Isfahan University of Technology, Iran

**S. V. Mirmoghtadaie**  
Isfahan University, Iran

In this paper a suitable method is presented which allows removing the spurious pass-bands of a parallel coupled-line bandpass filter. This configuration is constructed by applying wiggly line perturbation to the ground plane slot widths. First ground-plane slot dimensions are optimized for compensating the unequal modal electrical lengths using a commercially available electromagnetic simulator IE3D [1]. Using this method the double frequency spurious band associated with unequal even/odd electrical lengths can be suppressed or meaningfully reduced [2], then the slot widths is modulated with sinusoidal perturbations. The periods of the sinusoidal perturbations are selected according to desired spurious bands that must be rejected. Finally, in essential conditions, only the widths, gaps spacing and lengths of the coupled-line filter may be optimized to overcome the first passband perturbation. If the sinusoidal perturbations are applied to strip widths the first passband may be perturbed and optimization of coupled line dimensions is difficult [3]. With the proposed method undesired harmonic passbands of the filter are rejected. In addition optimization of coupled line dimensions is done easily.

## REFERENCES

1. Zeland Software Inc., IE3D Manual, 2004.
2. Velázquez-Ahumada, M. D. C., J. Martel, and F. Medina, “Parallel coupled microstrip filters with ground-plane aperture for spurious band suppression and enhanced coupling,” *IEEE Trans. Microwave Theory and Techniques*, Vol. MTT-52, 1082–1086, Mar 2004.
3. Nerukh, A., P. Sewell, and T. M. Benson, “Volterra integral equations for nonstationary electromagnetic processes in time-varying dielectric waveguides,” *J. of Lightwave Techn.*, Vol. 22, No. 5, 1408, 2004.
4. Lopetegi, T., M. A. G. Laso, F. Falcone, F. Martin, J. Bonache, J. Garcia, L. Pérez-Cuevas, M. Sorolla, and M. Guglielmi, “Microstrip “wiggly-line” bandpass filters with multispurious rejection,” *IEEE Microwave Wireless Compon. Lett.*, Vol. 14, 531–533, Nove 2004.

# Design of a Non-uniform High Impedance Surface for a Low Profile Antenna

M. Hosseini<sup>2</sup>, A. Pirhadi<sup>1,2</sup>, and M. Hakkak<sup>1,2</sup>

<sup>1</sup>Tarbiat Modares University, Iran

<sup>2</sup>Iran Telecommunication Research Center (ITRC), Iran

**Abstract**—Two Non-Uniform High Impedance Surfaces (NU-HIS or tapered HIS) are proposed against a Uniform HIS (U-HIS). All surfaces are one dimensional (1D) and made of parallel wires with a length a little less than  $\lambda/2$  around the resonance frequency. To show the effect of the surfaces, a half wavelength dipole antenna is placed over four different surfaces, PEC, U-HIS, NU-HIS, and modified NU-HIS (MNU-HIS) while the dipole height is fixed and very close to the surface. These four EM problems are analyzed numerically by the method of moments (MoM), and the results are compared. It is concluded that MNU-HIS yields more bandwidth than NU-HIS, and also, NU-HIS yields more bandwidth than U-HIS, while overall structures in all cases have identical volumes and nearly identical gains. This effect is attributed to the decrease of sensitivity to the angle of incidence by applying non-uniformity.

## 1. Introduction

It is well known that a high impedance surface or specifically a hypothetical perfect magnetic conductor may be very useful in a large variety of microwave and antennas applications. Recently, electromagnetic bandgap (EBG) structures have been widely studied for their behavior as High Impedance Surface (HIS) or Artificial Magnetic Conductor (AMC). Principally, they show stop band frequencies in which the tangential magnetic fields are considerably reduced. AMC is a special member of HIS family, which is designed to imitate the behavior of a perfect magnetic conductor (PMC). In fact, the AMC condition is characterized by the frequencies where the phase of the reflection coefficient is zero, i.e.,  $\Gamma = +1$  [1]. In contrast, a HIS may deviate a little from this condition, sometimes yielding more flexibility in antenna design. For example, in [2], the mushroom structure played the role of a ground plane for a dipole antenna a little upper than its resonance or AMC condition. Besides, in [3] the behavior of the same structure as a reactive impedance surface (RIS) was introduced, and the idea was applied to patch and dipole antennas. Repeatedly, it has been shown that HIS structures improve antenna performance and reduce the effects of surface waves. The latter feature yields better antenna radiation pattern and less coupling between elements of an array [2, 4]. So far, some 3D [5] and 2D [1, 3] structures have been proposed to realize HISs. Current realizations of 2D HISs are based on a planar FSS at the interface of a metal-backed dielectric slab with or without vertical vias [6]. This configuration is desirable because it is low-cost and easy to integrate in practice [7]. There is a problem with most of proposed HISs, however. In fact, the shift of the resonant frequency versus the incidence angle affects the performance of most well known HISs [8, 9]. To clarify this flaw, the behavior of a typical mushroom structure for different angles of incidence is presented in Fig. 1.

The curve has been obtained by Ansoft's Designer software, which is an electromagnetic solver based on MoM (equipped with Periodic MoM, PMM [1]). Generally, if the frequency bandwidth of low-profile antennas, placed near a typical HIS is within the resonance band of HIS, a significant improvement in the radiation efficiency is expected, compared to the conventional cases using PEC ground plane. However, the improvement is not always as much as desired [10]. An explanation for this behavior is that the high-impedance surface does not exhibit uniform surface impedance with respect to the different spatial harmonics radiated by an antenna, as depicted in Fig. 1. For instance, it is known that electrically small horizontal antennas radiate a large angular spectrum of TE and TM-polarized plane waves. As a result, the resonant frequency at which the effect of the magnetic wall is observed depends on the incidence angle; Therefore, the total interaction between the antenna and the HIS will be a summation of constructive and destructive effects [6].

References [1, 6, 7, 9, 11] are examples of the works concentrating completely on designing angularly stable HISs or AMCs. In all of these cases, the basic cell shape is changed and optimized, while the cell size is fixed throughout the structure (uniformly periodic structures). In the present work, we seek angular stability for HIS in order to improve antenna radiation near the surface. This is done by applying non-uniformity to a uniform HIS. Two 1D NU-HISs made of parallel wires are proposed, and their behaviors are compared with that of the uniform version (U-HIS). Then, the performance of a half wavelength dipole very close to all of these surfaces

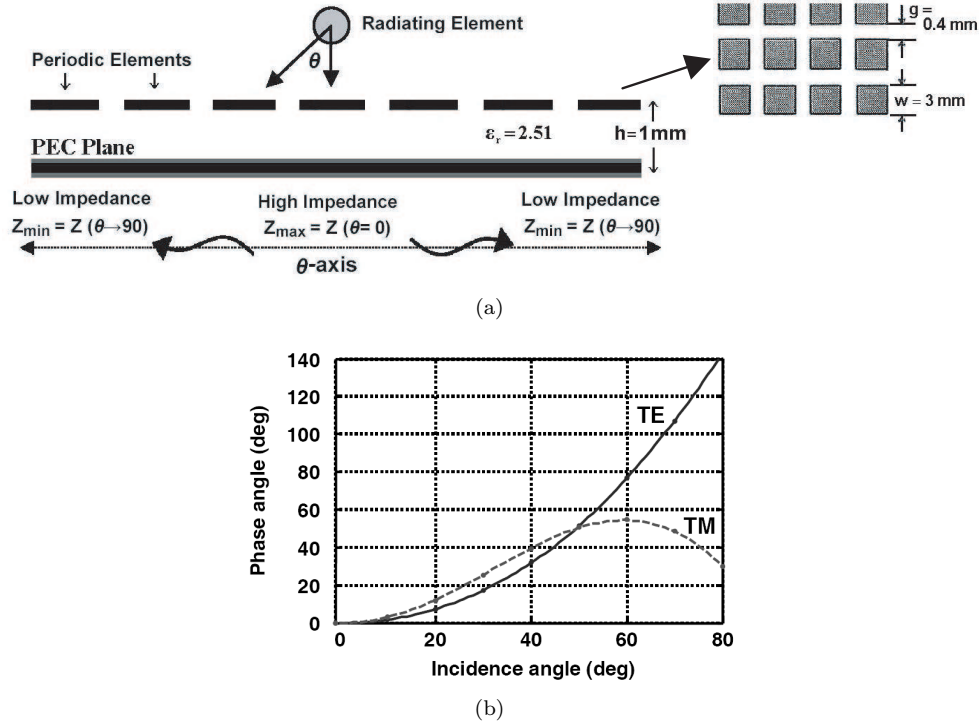


Figure 1: Behavior of a typical mushroom structure in different angles of incidence,  $f = 18.55$  GHz, a) front view, cross section, and the relevant dimensions, b) phase of reflection coefficient versus angle of incidence obtained by Ansoft's Designer software.

is investigated. During the process, as shown in Fig. 2, the dipole length and radius ( $\approx 0.45\lambda$  &  $\lambda/220$ ), the spacing of side elements from center ( $\approx 0.23\lambda$ ), and the spacing of dipole from the lower section of the planes (PEC planes) ( $\approx \lambda/12$ ) are kept fixed for better understanding of the influence of the surfaces alone. Because the structures are composed of wires, NEC software (NEC Win Pro. V 1.1), which is an electromagnetic solver based on MoM, is used for analysis.

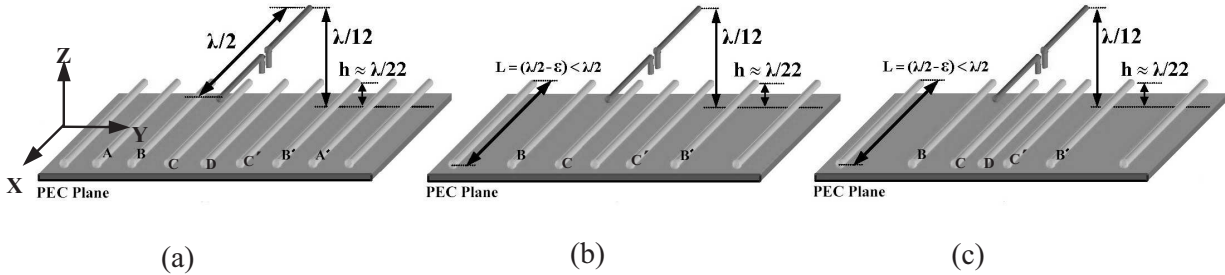


Figure 2: The geometry of the dipole antenna located over a) U-HIS, b) NU-HIS, and c) MNU-HIS.

## 2. The Main Idea, Explanation and Verification

The underlying basis for the idea in this paper returns to an important clue from this equation [12]:

$$\frac{X}{\eta_0} = F(p, w, \lambda) = \frac{p \cos \theta}{\lambda} \left[ \ln \left( \cos \operatorname{ec} \left( \frac{\pi w}{2p} \right) \right) + G(p, w, \lambda, \theta) \right] \quad (1)$$

where  $\eta_0$  and  $\lambda$  are free space wave impedance and wavelength respectively. Also,  $G$  is a correction term for large angles of incidence. The equation gives the surface impedance of parallel strips facing a TE plane wave as depicted in Fig. 3. Ignoring  $G$  in (1), the clue is that when  $w$  and  $\lambda$  are fixed,  $X$  can be kept stable by a proper increase of  $p$  against the increase of  $\theta$ . In other words, by gradually increasing  $p$  from center elements to the side ones (applying tapering), more angular stability is achievable. Note that the same effect is also attained by gradually decreasing  $w$ . But there are three problems in using such an idea. Firstly, as in Fig. 2, we have

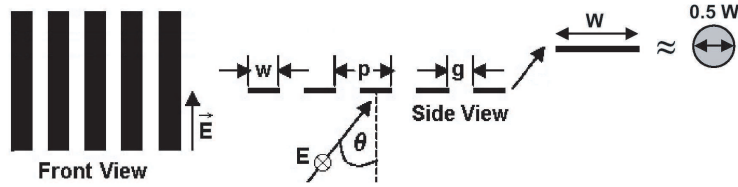


Figure 3: Front and side view of parallel metal strips (or equivalently wires) facing a TE plane wave impinging in different angles of incidence.

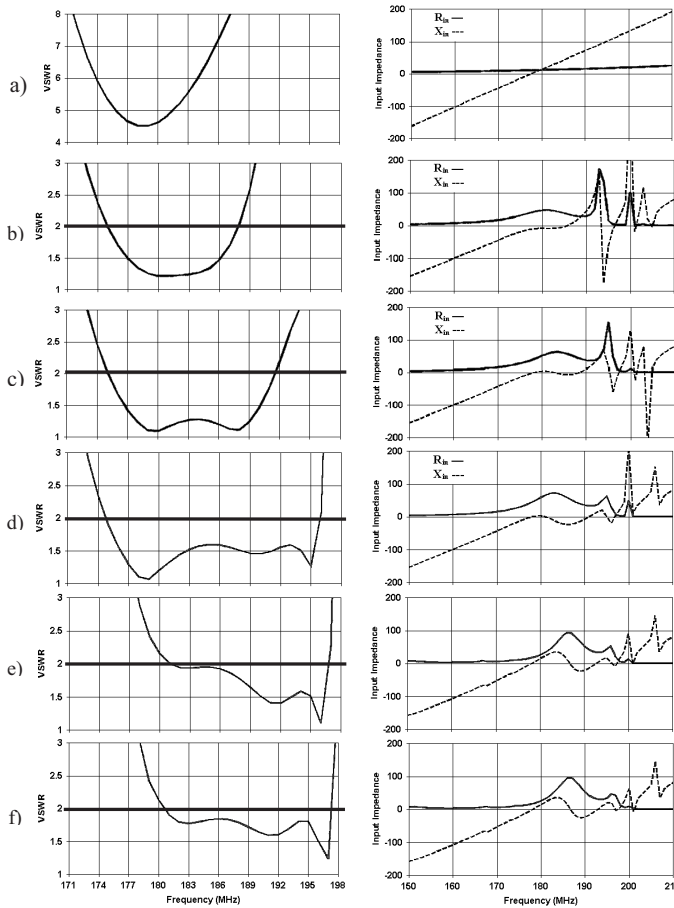


Figure 4: VSWR and input impedance of the dipole located over a) PEC ground plane, b) U-HIS, c) NU-HIS, d) MNU-HIS, e) MNU-HIS with finite wire ground plane, and f) the last design after a little tuning the dipole length and radius of side wires.

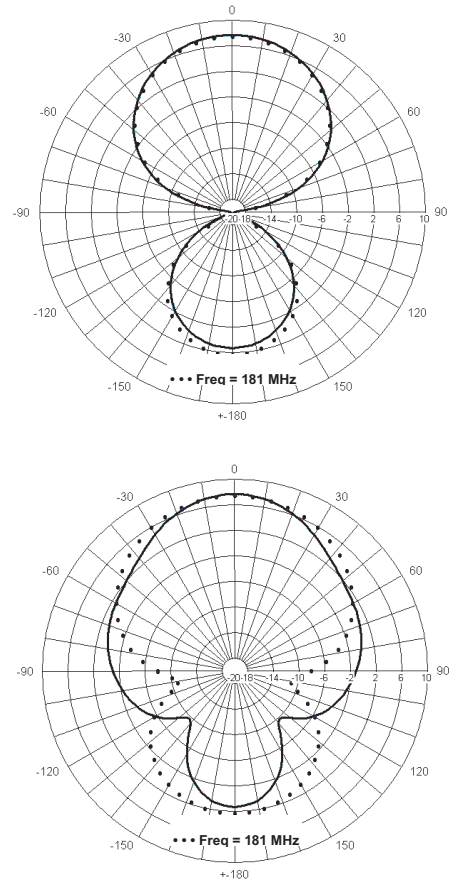


Figure 5: Gain (dB) for Fig. 2 (c), while the infinite PEC plane is replaced by the finite wire ground plane, a) E-plane, b) H-plane.

used parallel wires instead of strips; Secondly, (1) is not correct when the structure is placed near the PEC plane; Thirdly, in Fig. 3, the length of strips are infinite while those of this work are finite ( $\approx \lambda/2$ ). The first problem is solved considering the nearly equivalent scattering properties of strip and wire as depicted in Fig. 3 and stated in [6]. As for the second, it can be said that because here we need the general (not exact) effect of tapering on  $X$ , we can foresee that even in the present condition the general behavior in (1) remains true. Finally, as for the third, it is reminded from transmission line theory that a  $n\lambda/2$  slice of a transmission line represents an infinite line because the input impedance of such a line equals the load impedance. Fortunately, our numerical investigations have confirmed the correctness of the approximations and predictions above, at least for our proposed structures.

To study the effect of the idea, a half wavelength dipole antenna is numerically analyzed (by NEC) placed over four different surfaces, PEC, U-HIS, and NU-HIS, and modified NU-HIS (MNU-HIS) while the dipole

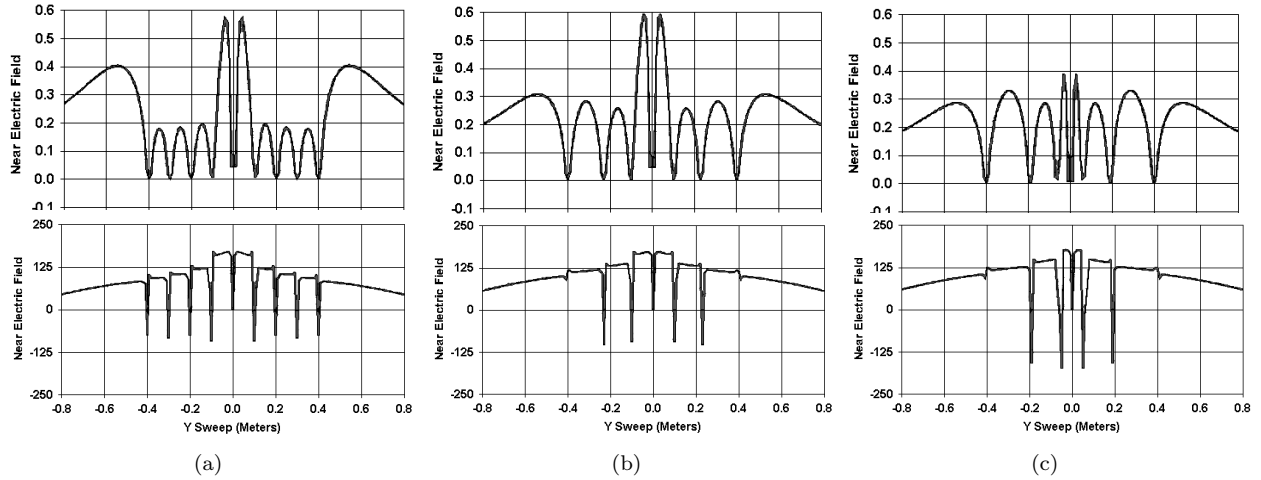


Figure 6: Near electric fields on the high impedance surfaces along  $Y$ -axis, excited by the dipole in Fig. 2,  $X = 0$ ,  $Z = 7.5$  cm,  $f = 184$  MHz, a) U-HIS (a), b) NU-HIS (b), and c) MNU-HIS (c) (upper row for amplitude and lower for phase of the fields).

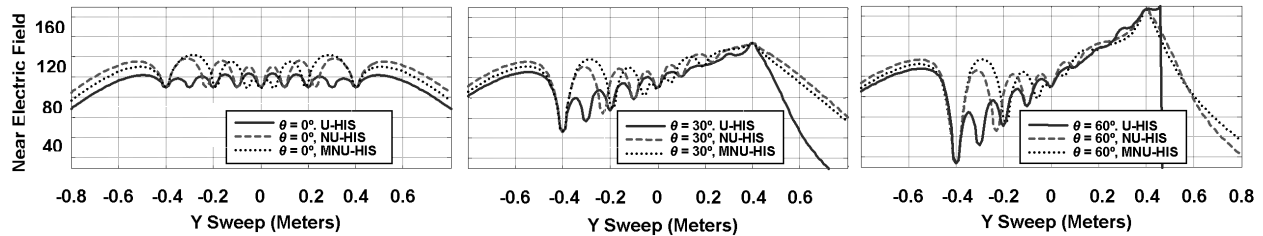


Figure 7: Phase of near electric fields excited by TE plane wave (in Fig. 2,  $E_X$ ) on the high impedance surfaces, along  $Y$ -axis,  $X = 0$ ,  $Z = 7.5$  cm,  $f = 184$  MHz.

height is fixed and very close to the surface. The proposed HISs are shown in Fig. 2 in which the dipole and the parasitic wires radii are 1 mm and 8 mm, respectively. As in Fig. 4 (a), for the dipole near the PEC plane without any parasitic wires, there is no resonance in  $Z_{in}$ . As a result, the VSWR is very poor. Deploying uniformly-placed wires ( $\approx \lambda/17.5$ ) close to the PEC plane ( $\approx \lambda/22$ ), as in Fig. 2 (a), a U-HIS is formed. As a result, the VSWR of the dipole will improve very much as in Fig. 4 (b). The bandwidth on VSWR ( $< 2$ ,  $Z_0 = 50$ ) is 6.3%. The curves are very similar to those in [2] and [3]. Now the non-uniformity idea emerging from (1) is applied by removing the two wires A and A' in Fig. 2 (a) and properly shifting the positions of B and B' sideways. The best result rendering the most bandwidth is a Non-Uniform HIS (tapered HIS) shown in Fig. 2 (b). Here the spacing BC is about  $\lambda/13.5$ . Fig. 4 (c) shows the VSWR and  $Z_{in}$  of this surface. As observed, the bandwidth increases from 6.3% to 9.3%. In the second step, considering the same point emerging from (1), it seems that also by making the center elements, C, D and C' a little denser the bandwidth may become better. Thus, using a simple optimization procedure, the spacing CD and simultaneously BC are adjusted in order to optimize the bandwidth on VSWR. The result is referred to as MNU-HIS and is shown in Fig. 2 (c). The spacing BC and CD are about  $\lambda/13$  and  $\lambda/29$  respectively. Fig. 4 (d) shows the related VSWR and  $Z_{in}$ . As seen, the bandwidth increases from 9.3% to 11.33%. Note that in all of these cases, the overall gain is nearly identical ( $\approx 9$  dB) while the overall structure volume is fixed (not including the PEC plane,  $0.45\lambda \times 0.45\lambda \times \lambda/12$ ).

Up to this point, all of the presented designs used an infinite PEC plane. In the next step, this ideal plane is modeled in NEC as a real finite plane ( $x \approx 0.45\lambda$  &  $y \approx 0.63\lambda$ ). Therefore, the overall structure volume is ( $0.45\lambda \times 0.63\lambda \times \lambda/12$ ). The corresponding VSWR and  $Z_{in}$  are shown in Fig. 4 (e). As obvious, due to cutting the plane, the bandwidth deteriorates to 7.95%. To remove this descent, the radius of the side elements is tuned a little. In fact, from (1), it is deduced that gradually reducing the radius is an alternative means of improving angular stability of the surface. This tuning is done simultaneously with a little tuning of the dipole length. After tuning, the best side elements radius is 7 mm (formerly 8 mm) and dipole length is 79.6 cm (formerly fixed at 80 cm). The improved result shows 9.45% bandwidth as in Fig. 4 (f). The relevant gains in E and H-planes

are depicted in Fig. 5. To give better understanding of the behavior of the surfaces, phase and amplitude of near fields excited by the dipole on the surfaces are presented in Fig. 6. In addition, the phases of near fields (on the surfaces) excited by a TE plane wave in different angles of incidence are rendered in Fig. 7. As deduced from Fig. 6, both the amplitude and phase become more stable as a result of imposing non-uniformity. In other words, in MNU-HIS the element right under the dipole and those on sides are illuminated much the same by the dipole. This is an implication for angular stability of the surface. Note that from apertures theory it is known that uniform phase and amplitude is an ideal condition yielding maximum performance. Fig. 7 is also a good indicator of angular stability of the surfaces. As observed, the phase of near fields on NUM-HIS withstands the most against increase of incidence angle. It can be concluded that the more the surface is angularly stable, the more bandwidth it renders near the dipole antenna. In other words, angular stability of the HIS, obtained through non-uniformity, improves the antenna performance.

### 3. Conclusion

The paper studies the effects of applying non-uniformity to a 1D uniform HIS. The proposed surfaces are made of parallel wires placed uniformly (U-HIS) or non-uniformly (NU-HIS) over a PEC ground plane. To show the effect of imposing non-uniformity, a half wavelength dipole antenna is numerically analyzed by MoM in the close vicinity of four different ground planes, PEC, U-HIS, NU-HIS, and modified NU-HIS (MNU-HIS), while the dipole height and length are kept fixed. Comparison of the results shows that MNU-HIS yields more bandwidth than NU-HIS, and also, NU-HIS yields more bandwidth than U-HIS, while all cases have identical volume and nearly identical gain. This effect is attributed to the improvement of angular stability of the surfaces caused by applying an apt non-uniformity.

### REFERENCES

1. Kern, D. J., D. H. Werner, A. Monorchio, L. Lanuzza, and M. J. Wilhelm, "The design synthesis of multi-band artificial magnetic conductors using high impedance frequency selective surfaces," *IEEE Transactions on Antennas and Propagation*, Vol. 53, No. 1, Jan. 2005.
2. Yang, F. and Y. Rahmat-Samii, "Reflection phase characterizations of the ebg ground plane for low profile wire antenna applications," *IEEE Transactions on Antennas and Propagation*, Vol. 51, No. 10, 2691–2703, Oct. 2003.
3. Mosallaei, H. and K. Sarabandi, "Antenna miniaturization and bandwidth enhancement using a reactive impedance substrate," *IEEE Transactions on Antennas and Propagation*, Vol. 52, No. 9, 2403–2414, Sep. 2004.
4. Li, Z. and Y. Rahmat-Samii, "PBG, PMC, and PEC ground planes: a case study of dipole antennas," *IEEE AP-S Symp. Dig.*, Vol. 2, 674–677, Jul. 2000.
5. Sievenpiper, D., L. Zhang, R. F. Jimenez Broas, N. G. Alexopolous, and E. Yablonovitch, "High impedance electromagnetic surfaces with a forbidden frequency band," *IEEE Trans. Microwave Theory Tech.*, Vol. 47, 2059–2074, Nov. 1999.
6. Simovski, C. R., P. de Maagt, and I. V. Melchakova, "High-impedance surfaces having stable resonance with respect to polarization and incidence angle," *IEEE Transactions on Antennas and Propagation*, Vol. 53, No. 3, March 2005.
7. Monorchio, A., G. Manara, and L. Lanuzza, "Synthesis of artificial magnetic conductors by using multi-layered frequency selective surfaces," *IEEE Antennas And Wireless Propagation Letters*, Vol. 1, 2002.
8. Simovski, C. R., S. A. Tretyakov, and P. de Maagt, "Artificial high-impedance surfaces: Analytical theory for oblique incidence," *Proc. Antennas Propag. Soc. Int. Symp.*, Vol. 4, 434–437, 2003.
9. Simovski, C. R., P. de Maagt, S. A. Tretyakov, M. Paquay, and A. A. Sochava, "Angular stabilization of resonant frequency of artificial magnetic conductors for TE-incidence," *Electron. Lett.*, Vol. 40, No. 2, 92–93, 2004.
10. G. Poilasne, "Antennas on high-impedance ground planes: On the importance of the antenna isolation," *Progress Electromagn. Res.*, Vol. PIER-41, 237–255, 2003.
11. Lanuzza, L., A. Monorchio, and G. Manara, "Synthesis of high-impedance fsss. using genetic algorithm," *Antennas and Propagation Society International Symposium*, Vol. 4, 364–367, June 2002.
12. Marcuvitz, N., *Waveguide Handbook*, McGraw Hill, 1951.

## Axial Focusing Properties of Cosine-Gaussian Beam by a Lens with Spherical Aberration

Q. F. Wang, X. Q. Wang, L. Wang, J. J. Lin, J. S. Tang, and K. Sheng  
Southwest Jiaotong University, China

Based on the expression for the axial light intensity of cosine-Gaussian beam by a lens with spherical aberration, the influence of the coefficient of the spherical aberration and Fresnel number of Gaussian beams on the axial intensity distribution is discussed. The numerical results show that for the lens with negative spherical aberration, near the best focal point, the axial light intensity changes slowly with the changing of propagation distance. So, the negative spherical aberration may be an approach for achieving the flattened laser intensity distribution along propagation axis. When the parameters of the beam and the optical system satisfy some conditions, there are two axial light intensity maxima which are located on both sides of the geometrical focus of focused cosine-Gaussian beam. For the lens without spherical aberration, the maximum light intensity, or the best focal point is on the left side of the geometrical focus. For the lens with positive spherical aberration, the best focal position can leap to the right side of geometrical focus,  $z_{f2}$  from the left of it,  $z_{f1}$ , when the value of Fresnel number of Gaussian beams  $N_w$  changes, it is so-called focal switch. With the increasing of the coefficient of the spherical aberration  $kS_1$ , relative transition height  $\Delta z_f = |z_{f1} - z_{f2}|$  increases, but the value of critical Fresnel number  $(N_w)_c$  decreases. For example, when the coefficient of the spherical aberration equals 0.5 and 0.3, and, the critical Fresnel number equals 7.03 and 8.68 (when the transition occurs), the relative transition height  $\Delta z_f$  equals 0.246 and 0.146 respectively. It is also shown that when the coefficient of the spherical aberration is small, the value of critical Fresnel number  $(N_w)_c$  decreases rapidly as the  $kS_1$  increases. After about  $kS_1 = 0.3$  the value of  $(N_w)_c$  decreases slowly.

# Some Applications of the High-mode-merging Method

J. Tang<sup>1</sup>, X. Wang<sup>1</sup>, L. Wang<sup>1</sup>, S. Cao<sup>1</sup>, Z. Wang<sup>2</sup>, J. Gao<sup>1</sup>, and K. Sheng<sup>1</sup>

<sup>1</sup> Southwest Jiaotong University, China

<sup>2</sup> NC A and T State University, USA

**Abstract**—Waves guided along dielectric step discontinuity can be described by a multi-port network [1] and it is simplified as a two-port network with the influence of high-modes retaining [2]. These results can be used for treat dielectric strip waveguide, even more complicated structures. Some numerical results are got for a strip and a groove dielectric waveguide some kind of resonant phenomena also is obtained. Some comments on this method and some suggestions are given furthermore.

## 1. Introduction

A dielectric strip waveguide can be seen as a system constituted by 2 step discontinuous structure as shown in Fig. 1. As a symmetric system, it also can be treated by so-called bisection method, namely, it can be see equivalently as the result of superposition of 2 networks with short circuit(sc) and open circuit(oc) separately at the terminals of transmissions of length  $l/2$  (Fig. 2) [1].

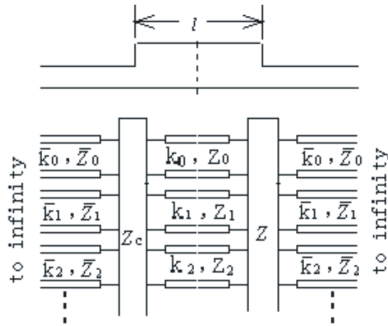


Figure 1: Network of a dielectric strip waveguide.

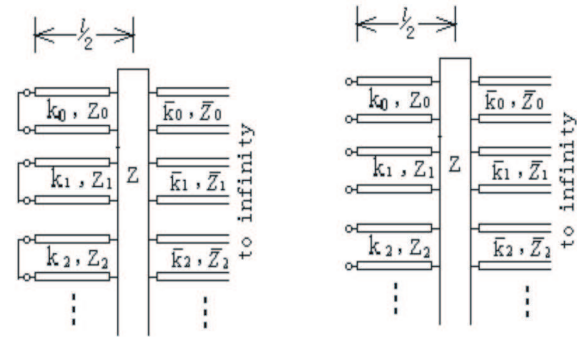


Figure 2: Bisection treatment of the dielectric strip waveguide.

This problem can be simplified by high-mode-merging method provide in [2], a two-port network in which the influence of high modes is considered has been obtained, but in present case, all  $Z_m$  in  $E, F, G$  and  $H$  of [2] ((17a-d) in [2] respectively) are replaced by

$$jZ_m \tan k_0(l/2) \quad (\text{for sc}) \tag{1}$$

$$-jZ_m \cot k_0(l/2) \quad (\text{for oc}) \tag{2}$$

There are three methods to treat the problem of strip waveguide.

## 2. Equivalent Circuit Method

As most of microwave engineers are more familiar to the circuit language, the network is realized by a simple  $T$  circuit generally, (see Fig. 3), impedances of which,  $Z_a, Z_b$  and  $Z_c$  are related to elements of  $Z$ -matrix,  $Z_{11}Z_{12}Z_{21}$  and  $Z_{22}$  by

$$Z_a = Z_{11} - Z_{12} \quad Z_b = Z_{22} - Z_{12} \quad Z_c = Z_{12}(= Z_{21}) \tag{3}$$

(see appendix) and also be distinguished for sc and oc. In present case, we have Fig. 4(a), the impedances looking left into the network at 2-2' plane in two cases are

$$Z_{in}^{sc} = Z_b^{sc} + \frac{Z_c^{sc}(Z_a^{sc} + Z_{in,0}^{sc})}{Z_c^{sc} + Z_a^{sc} + Z_{in,0}^{sc}} \quad (\text{for sc}) \tag{4a}$$

$$Z_{in}^{oc} = Z_b^{oc} + \frac{Z_c^{oc}(Z_a^{oc} + Z_{in,0}^{oc})}{Z_c^{oc} + Z_a^{oc} + Z_{in,0}^{oc}} \quad (\text{for oc}) \tag{4b}$$

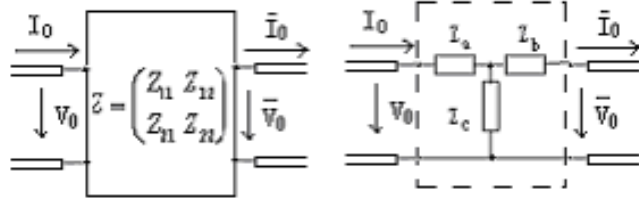


Figure 3: The comparison of a network and a circuit.

where  $Z_{in,0}^{sc}$  and  $Z_{in,0}^{oc}$  are the input impedances at 1-1' plane looking left into transmission line with length  $l/2$  in sc and oc cases, which can be got by (1a) and (1b) respectively.

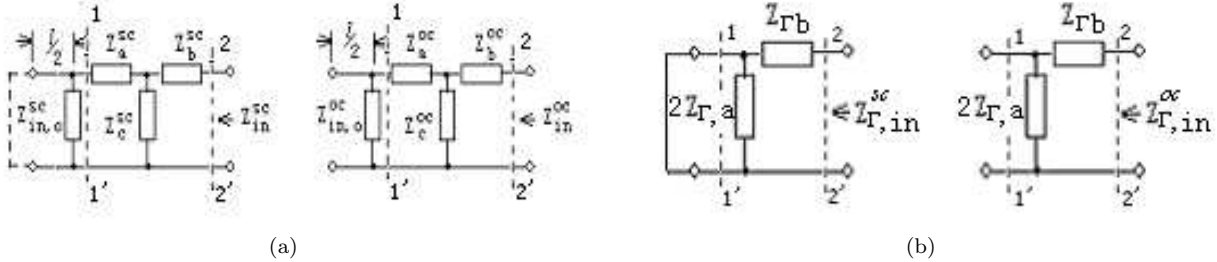


Figure 4: a) T-circuit b) Γ-circuit.

The system in Fig. 4(a) also can be changed to a Γ-circuit as shown in Fig. 4(b). Obviously,

$$Z_{\Gamma,in}^{sc} = Z_{\Gamma,b} \tag{5a}$$

$$Z_{\Gamma,in}^{oc} = Z_{\Gamma,b} + 2Z_{\Gamma,m} \tag{5b}$$

Let them be equivalent, i.e., we have  $Z_{T,in}^{sc} = Z_{\Gamma,in}^{sc}$  and  $Z_{T,in}^{oc} = Z_{\Gamma,in}^{oc}$ , then,

$$Z_{\Gamma,b} = Z_{\Gamma,in}^{sc} = Z_{T,in}^{sc} \tag{6a}$$

$$Z_{\Gamma,m} = (Z_{\Gamma,in}^{oc} - Z_{\Gamma,b})/2 = (Z_{T,in}^{oc} - Z_{T,in}^{sc})/2 \tag{6b}$$

where  $Z_{T,in}^{sc}$  and  $Z_{T,in}^{oc}$  are given by (4a) and (4b) respectively. A strip dielectric waveguide can be seen as a combination of two Γ-circuits which connected back to back as shown in Fig. 5(a), then it can be reformed as Fig. 5(b). Going back to network, the elements of a strip waveguide can be got by (3a) and (3b) in opposite way.

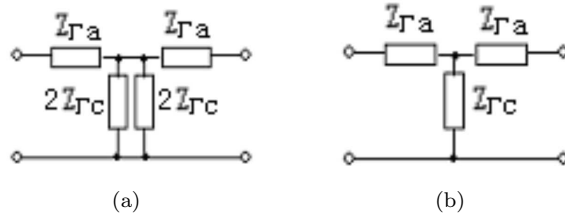


Figure 5: (a) Combination of two Γ-circuits (b) Its deformation.

### 3. Equivalent Network Method

A little bit different approach is called equivalent network method (EN method). The elements of Z-matrix can be normalized as follows.

$$Z'_{11} = Z_{11}/Z_0 \quad Z'_{12} = Z_{12}/\sqrt{Z_0 Z_0} \tag{7a}$$

$$Z'_{21} = Z_{21}/\sqrt{Z_0 Z_0} \quad Z'_{22} = Z_{22}/Z_0 \tag{7b}$$

Considering the high-mode=merging method, we have

$$Z'_{11} = \left(\frac{F}{H}\right)/Z_0 \quad Z'_{12} = \left(E + \frac{GF}{H}\right)/\sqrt{Z_0\bar{Z}_0} \tag{8a}$$

$$Z'_{21} = \left(\frac{1}{H}\right)/\sqrt{\bar{Z}_0Z_0} \quad Z'_{22} = \left(\frac{G}{H}\right)/\bar{Z}_0 \tag{8b}$$

Where  $E, F, G$  and  $H$  are given in [2], and the determinate of normalized Z-matrix

$$\text{Det } Z' = Z'_{11}Z'_{22} - Z'_{21}Z'_{12} = \frac{E}{H}/(Z_0\bar{Z}_0)$$

then we can get the transfer matrix for right step discontinuity of the strip waveguide

$$A'_r = A' = \frac{1}{Z'_{21}} \begin{bmatrix} Z'_{11} & |Z'| \\ 1 & Z'_{22} \end{bmatrix} = \begin{bmatrix} F\sqrt{\bar{Z}_0/Z_0} & -E/\sqrt{Z_0\bar{Z}_0} \\ H\sqrt{Z_0\bar{Z}_0} & G/\sqrt{Z_0\bar{Z}_0} \end{bmatrix} \tag{9}$$

Let voltage and current in both sides of the right discontinuity be normalized as

$$V'_0 = V_0/\sqrt{\bar{Z}_0}, I'_0 = I_0\sqrt{\bar{Z}_0}, \bar{V}'_0 = \bar{V}_0/\sqrt{\bar{Z}_0}, \bar{I}'_0 = \bar{I}_0\sqrt{\bar{Z}_0}$$

Then we have

$$\begin{bmatrix} V'_0 \\ I'_0 \end{bmatrix} = A'_r \begin{bmatrix} \bar{V}'_0 \\ \bar{I}'_0 \end{bmatrix}$$

Considering symmetry of the strip, the matrix of left step discontinuity is just the inverse matrix of one of the right step:

$$A'_l = (A'_r)^{-l} (= (A')^{-l}) = \begin{bmatrix} G\sqrt{\bar{Z}_0/Z_0} & H/\sqrt{Z_0\bar{Z}_0} \\ -E\sqrt{Z_0\bar{Z}_0} & F/\sqrt{Z_0\bar{Z}_0} \end{bmatrix} \tag{10}$$

The uniform structure between two step discontinuities corresponds a segment of an uniform transmission line with length  $l$ , the transfer matrix of which is

$$A'_m = \begin{bmatrix} \cos k_0l & j \sin k_0l \\ j \sin k_0l & \cos k_0l \end{bmatrix} \tag{11}$$

Finally, the transfer matrix of the whole strip can be got as the continued-multiplication product:

$$A'_{strip} = A'_l A'_m A'_r = (A')^{-1} A'_m A' \tag{12}$$

This procedure can be shown in Fig. 6(a). For a rectangular groove dielectric waveguide, corresponding matrix, then, is

$$A'_{groove} = A' A'_m (A')^{-1} \tag{13}$$

(see Fig. 6(b)).

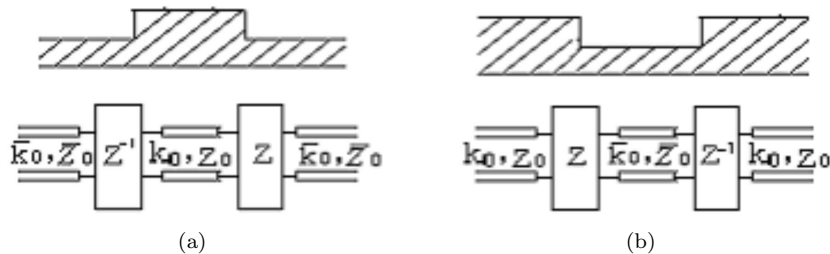


Figure 6: (a) Strip waveguide (b) Groove waveguide .

### 4. Effective Dielectric Constant Method

Besides there is also a rather rough method, in which the influence of all high-modes is neglected, that we only take the  $A'_m$  as the transfer matrix of whole strip (or groove waveguide):

$$A'_{strip} = A'_m \tag{14}$$

It's so-called effective dielectric constant (EDC) method.

### 5. Numerical Examples

For comparing these 3 methods, some numerical calculations have been done for some characteristics of some kinds of waveguides: Fig. 7(a)–(c) show plots of reflection and transmission coefficients (including the argument and modulus both of them) vs width of waveguide; Fig. 7(d) gives ones for loss.

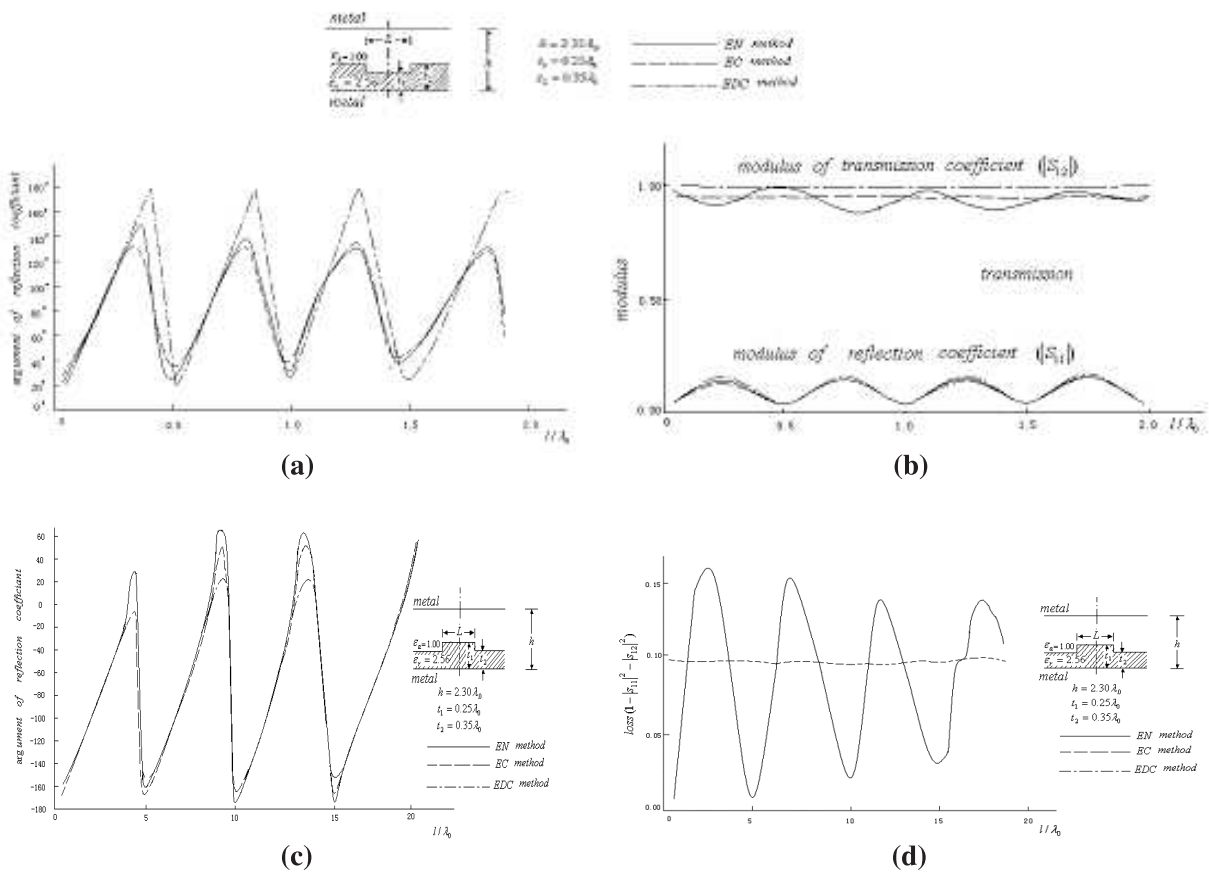


Figure 7: Some numerical results.

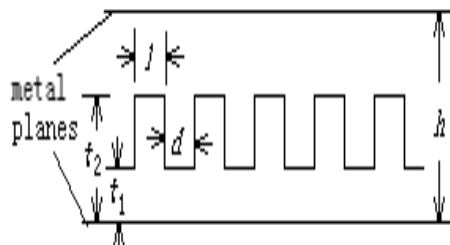


Figure 8.

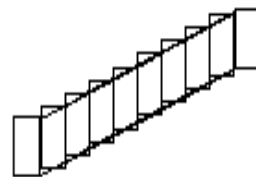


Figure 9.

## 6. Conclusion

- (1) The results for all methods give similar tendency and accord one another pretty good in certain accuracy; especially results of EN method and EC method are more closed.
- (2) The EDC method is still useful in some cases because it is rather simple and easy for calculations and with clear physical meaning. A significant defect is that it can't give the loss.
- (3) There is some kind of periodic phenomena existing. The reflection coefficients, both argument and modulus, and loss are varying with the width of waveguide periodically. It is coincide with the conclusion of [3]. This phenomena can be seen as resonance, but the mechanism of it is remained to be explained further. It is also indicated that the high-mode-merging method is correct.
- (4) In high-mode-merging method, the coupling between TE modes and TM-modes has not been considered. It is also one of the defects of this theory.
- (5) In the original theory of [1], two parallel perfect conductive planes are needed. So, the waveguide discussed here is not open absolutely. If the upper one of them moved far enough, it almost can be seen as an open one approximately. If we want to remove the upper conductive plane, we'll get infinite number of continuous high modes it is a problem of continuous spectrum and is out of the topic of this paper.
- (6) The cascade network method is not confined to solve only symmetric system like single strip dielectric waveguide but also can be extended to treat some more complicated structures, such as finite periodic strip(groove) dielectric waveguide (Fig. 8), the curved surface dielectric waveguide (Fig. 9) etc.

## Appendix

Consider a T-circuit as shown in Fig. 3. The transfer matrixes of Fig. 3 devices are

$$A_a = \begin{bmatrix} 1 & Z_a \\ 0 & 1 \end{bmatrix}, \quad A_c = \begin{bmatrix} 1 & 0 \\ 1/Z_c & 1 \end{bmatrix}, \quad A_b = \begin{bmatrix} 1 & Z_b \\ 0 & 1 \end{bmatrix}$$

As a whole, the transfer matrix then is

$$A = A_a A_c A_b = \begin{bmatrix} 1 + Z_a/Z_c & Z_a + Z_b + Z_a Z_b/Z_c \\ 1/Z_c & 1 + Z_b/Z_c \end{bmatrix} = \begin{bmatrix} a & b \\ c & d \end{bmatrix}$$

where  $a = 1 + Z_a/Z_c$ ,  $b = Z_a + Z_b + Z_a Z_b/Z_c$ ,  $c = 1/Z_c$ , and  $d = 1 + Z_b/Z_c$  with  $|A'| = ad - bc = 1$ . Then, changing it to impedance matrix equivalently, we get

$$Z = \frac{1}{c} \begin{bmatrix} a & |A'| \\ 1 & d \end{bmatrix} = \begin{bmatrix} Z_a + Z_c & Z_c \\ Z_c & Z_b + Z_c \end{bmatrix} = \begin{bmatrix} Z_{11} & Z_{12} \\ Z_{21} & Z_{22} \end{bmatrix}$$

Namely, we get

$$Z_{11} = Z_a + Z_c \qquad Z_{12} = Z_{21} = Z_c \qquad Z_{22} = Z_b + Z_c$$

## REFERENCES

1. Peng, S. T. and A. A. Oliner, "Guidance and leakage properties of a class of open dielectric waveguides: part I—mathematics formulation," *IEEE Trans. on MTT*, Vol. MTT-29, 843–855, Sept. 1981.
2. Tang, J. S., K. M. Sheng, and J. Gao, "The high-mode-merging technique for dielectric waveguides," *Proc. of PIERS 2005*, Hangzhou, China, 142–146, Aug. 2005.
3. Peng, S. T., A. A. Oliner, I. T. Hsu, and A. Sanches, "Guidance and leakage properties of a class of open dielectric waveguides: part II—new physical effects," *IEEE Trans. on MTT*, Vol. MTT-29, 855–869, Sept. 1981.

# Analysis of Circular Cavity with Metalized Dielectric Posts or Corrugated Cylinders

R. Lech and J. Mazur

Gdansk University of Technology, Poland

This paper presents the analysis of electromagnetic wave scattering by cylindrical objects located arbitrarily in a circular cavity. The general configuration of the resonators to be investigated is shown in Figure 1. The posts structures can be either homogenous along the height of the resonator or homogenous along their circumference. The first kind of posts is composed of metalized dielectric, cylindrical rod or fragments of metallic cylinder as depicted in Fig. 1(a), while the latter is a corrugated metallic cylinder (see Fig. 1(b)). The proposed structures can be utilized as a key building elements of combine and tunable filters and measurements resonators.

In both cases the exact full-wave theory based on the mode-matching method is applied to analyze the structures. Both TE and TM modes are considered simultaneously in the analysis. Additionally, to eliminate the phenomenon of relative convergence when sharp metallic edges are presents, the analysis includes the edge condition. A set of integral equations in the tangential electric fields at the interfaces are derived and solved with the use of the basis functions which contain as much as possible information on the behavior of these fields at all sharp metallic edges [1, 2].

This ensures numerical efficiency and fast convergence of the method. The resonance frequencies of the investigated resonators are accurately determined. Validity and accuracy of the approach will be verified by comparing the results with Quick Wave FDTD Simulator, FEM method and experiment. A good agreement with FDTD method for a couple examples was obtained and presented in the tables below.

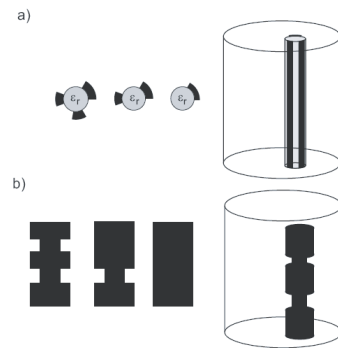
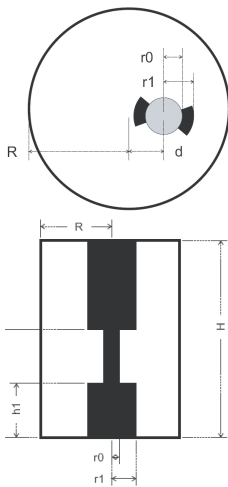


Figure 1: Analyzed structure. a) metalized dielectric, cylindrical post in circular cavity; b) corrugated metallic cylinder in circular cavity.



Data:  $r_0 = 5\text{mm}$ ;  $r_1 = 10\text{mm}$ ;  $R = 30\text{mm}$ ;  $H = 100\text{mm}$ ;  $d = 0\text{mm}$  and  $d = 10\text{mm}$ ; the resonance frequencies are in GHz

$d = 0\text{mm}$			$d = 10\text{mm}$		
p	Our Results	FDTD Method	p	Our Results	FDTD Method
0	6.21	6.23	0	5.389	5.398
	6.541	6.565		6.456	6.470
	7.582	7.598		7.056	7.067
1	6.362	6.382	1	5.589	5.597
	6.697	6.718		6.620	6.637
	7.728	7.747		7.162	7.169
2	6.779	6.797	2	6.148	6.150
	7.142	7.154		7.088	7.067
	8.152	8.166		7.446	7.450

Data:  $r_0 = 5\text{mm}$ ;  $r_1 = 10\text{mm}$ ;  $R = 30\text{mm}$ ;  $H = 100\text{mm}$ ;  $d = 0\text{mm}$  and  $d = 10\text{mm}$ ;  $h_1 = 20\text{mm}$ ;  $h'_1 = 40\text{mm}$ ; the resonance frequencies are in GHz

$d = 0\text{mm}$		$d = 10\text{mm}$	
Our Results	FDTD Method	Our Results	FDTD Method
2.880	2.895	2.894	2.904
3.960	3.945	2.994	3.020
4.930	4.922	3.964	3.961
		4.036	4.035
		4.838	4.820
		4.842	4.834

## REFERENCES

- Amari, S., S. Catreux, R. Vahldieck, and J. Bornemann, "Analysis of ridged circular waveguides by the coupled-integral-equations technique," *IEEE Transaction on Microwave Theory and Techniques*, Vol. 46, No. 5, May 1998.
- Lech, R., M. Polewski, and J. Mazur, "Scattering in junction by posts consisting of a segment of conducting cylinder," *IEEE Transaction on Microwave Theory and Techniques*, Vol. 51, No. 3, 998–1002 March 2003.

# UWB Textile Antennas for Wearable Applications

M. Klemm and G. Troester

Swiss Federal Institute of Technology, Switzerland

Wearable computing is a new, fast growing field in application-oriented research. Steadily progressing miniaturization in microelectronics along with other new technologies enables wearable computing to integrate functionality in clothing allowing entirely new applications. Integration in textiles ideally combines such requirements since clothing offers unobtrusiveness, a large area and body proximity. However, such electronic devices have to meet special requirements concerning wearability. Ultra-wideband (UWB) is an emerging wireless technology, recently approved by FCC. In low/medium data-rate applications, like wearable computing, UWB offers low-power operation and extremely low radiated power, thus being very attractive for body-worn, battery-operated devices.

In this paper we present new ultra-wideband (UWB) textile antennas for wearable applications. These antennas are made entirely of textiles. As a conductor we have used metalized textile with the surface resistivity of  $0.1 \Omega/\text{sq.}$ , which offer low ohmic losses. As the dielectric substrate, very thin (0.5 mm) textile with dielectric constant 2.6 (extracted from measurements). This textile dielectric was chosen due to a relatively high dielectric constant and a small thickness. Prior textile antennas (e.g., [Klemm, EuMW 2004]) were usually composed of dielectric materials with  $\epsilon_r$  only slightly higher than 1, and thicknesses of 4–6 mm. Therefore, a new feature of our antennas is that they could be easily integrated directly into clothing, rather than being attached.

We have realized different types of thin UWB textile antennas, both in microstrip and coplanar (CPW) techniques. To our best knowledge, these are the first CPW-fed textile antennas reported in the open literature.

Due to the limited space, in Fig. 1(a) we present only one example of the manufactured UWB textile antenna: CPW-fed textile UWB disc monopole antenna. In Fig. 1(b) we compare measured (two prototypes) and simulated return loss (RL) characteristics, which agree relatively well. Both measured antennas have RL below 10dB from 3.4 GHz to 10.2 GHz.

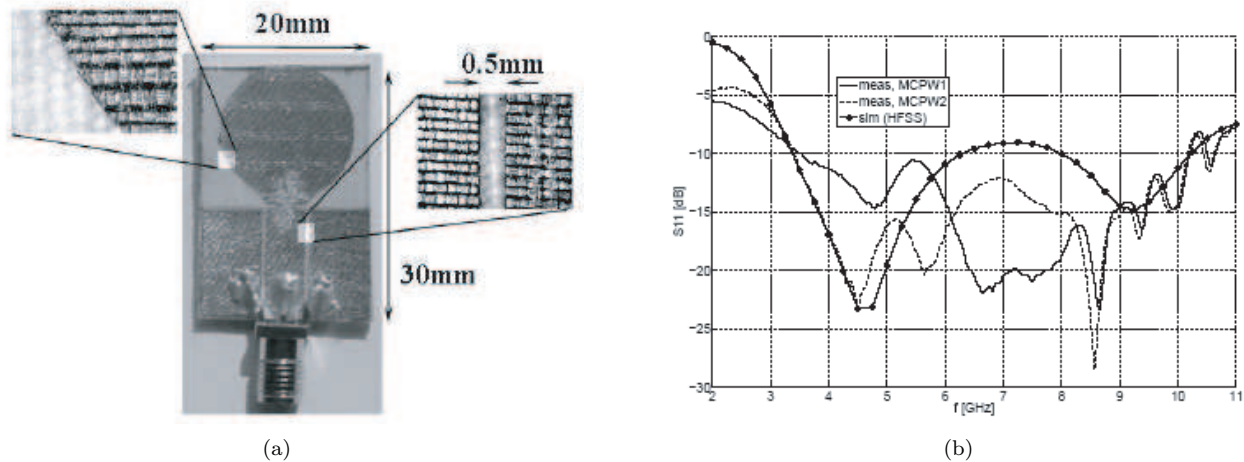


Figure 1: The CPW-fed UWB disc monopole antenna: a) photo, b) Measured (two realizations) and simulated return loss characteristics.

## Propagation of Strong Electromagnetic Waves in Semiconductors with S-shaped Current Voltage Characteristics

Y. G. Gurevich and J. E. Velázquez-Pérez  
Universidad de Salamanca, Spain

It is well known that some semiconductors exhibit a S-shaped dependence of the electron temperature with the local electric field. Usually such dependence leads to the same kind of dependence in the current-voltage characteristics [1, 2].

In this work we will present the theory of the propagation of strong electromagnetic waves in such media. In our study we have found that a semi-infinite semiconductor when excited with a strong electromagnetic wave will exhibit an internal discontinuity of the electrical permittivity. The position of this discontinuity is found to be a function of the magnitude of the electromagnetic wave ( $E_0$ ).

From the an application point of view, this property can be exploited to design a Fabry-Pérot interferometer. The thickness of this interferometer can be modulated by  $E_0$ . As a consequence of the above described, the reflectance value will exhibit an oscillatory dependence with the magnitude of the electromagnetic wave.

### REFERENCES

1. Volkov, A. F. and S. M. Kogan, *Sov. Phys. Uspek.*, Vol. 96, 633, 1968.
2. Baas, F. G. and Y. G. Gurevich, *Sov. Phys., JETP*, Vol. 28, 572, 1969.

# Effect of Surface Defects on the Amplification of Anomalous Transmission in Dielectric and Metallic Photonic Band Gap Materials: Calculation and Experimental Verification

S. Massaoudi, A. Ourir, and A. de Lustrac  
 Université Pairs-Sud, France

We study the distribution of defects on dielectric and metallic Photonic Band Gap materials. We'll show that the surface defects lead to the amplification of anomalous transmission and excitation of the new electromagnetic modes. These properties allow very interesting applications, such as controlable antennas with high directivity, or compact demultiplexer for WDM [1]. The dielectric and metallic PBG-prisms, which we studied are made of dielectric or metallic rods disposed in an isosceles right-angled triangle.

## The Results of the Dielectric PBG-prism

The Fig. 1(a) shows the radiation pattern measured at 16 GHz of a prism without defect.

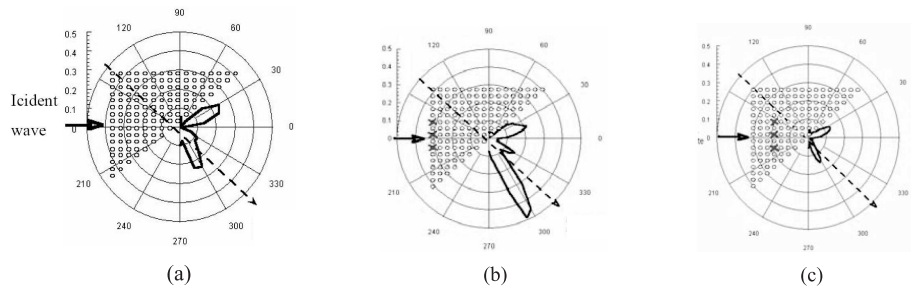


Figure 1: Measured near field radiation pattern at 16 GHz. a) Perfect PBG-prism, b) The PBG-prism with three cavities (in red) placed on the surface, and c) The PBG-prism with three defects inside.

The Fig. 1(b) gives the radiation pattern measured at 16 GHz of a prism with three defects on the surface of the dielectric. The Fig. 1(c) shows the radiation pattern measured at the at 16 GHz of a prism with three defects inside.

## The Results of Metallic PBG-prism

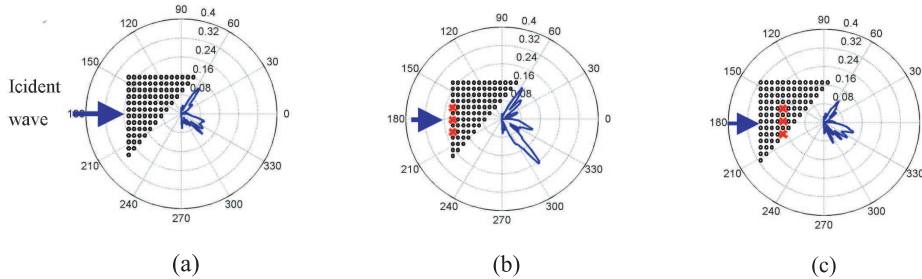


Figure 2: Measured near field radiation pattern at 12 GHz of metallic PBG-prism. a) Perfect PBG-prism, b) The PBG-prism with three cavities (in red) placed on the surface, and c) The PBG-prism with three defects inside.

The Fig. 2(a) shows the radiation pattern measured at 12 GHz of a prism without defect. The Fig. 2(b) gives the radiation pattern measured at 12 GHz of a prism with three defects on the surface of the dielectric. The Fig. 2(c) shows the radiation pattern measured at the at 12 GHz of a prism with three defects inside.

## REFERENCES

1. Lustrac, A. de, T. Brillat, F. Gadot, and E. Akmansoy, "The use of controllable photonic band gap (CPBG) materials: an antenna application," *Optical-and-Quantum-Electronics*, Vol. 34, Nos. 1-3, 265, January-March 2002.

# Dielectric Waveguide Filter with Cross Coupling

D. S. Jun, H. Y. Lee, D. Y. Kim, S. S. Lee, E. S. Nam, and K. I. Cho  
 Electronics and Telecommunications Research Institute, Korea

Recently, commercial millimeter wave applications such as 60 GHz communication systems or 77 GHz autonomous cruise control highly require surface mountable planar millimeter wave bandpass filters with a narrow bandwidth for low cost and compact integration of RF (Radio Frequency) front-ends. Metallic rectangular waveguide filters result in high production costs and bulky integration to planar circuits.

In this paper, we describe newly developed three resonator dielectric waveguide filters. The reduction in the number of resonators contributes to the compact, which is smaller than the previous three resonator dielectric waveguide filters. To improve stop band rejection for filters with a smaller number of resonators, cross coupling between 1st and 3rd resonators is introduced by twodimensional arrangement of resonators, which provides an attenuation pole at the higher frequency side of the pass band. The coupling between resonators is introduced by three-dimensional arrangement of resonators, which expect low cost and compact integration of RF front-end modules.

The waveguide structure is by forming metallized through holes in a dielectric substrate with metallized surfaces. In order to cross coupling for attenuation pole, the resonators are arranged twodimensionally. The structure facilitates realization of cross coupling by the space between though holes. *T*-shaped waveguide to GCPW (Ground Coplanar Waveguide) transitions lead to input/output ports, which enable flip chip bonding or external system probe connecting. The space between though holes around the input/output port must be sufficiently narrow to avoid propagation of the waveguide mode within the waveguide because a wide spacing can cause unwanted coupling. Also, the space between though holes of the waveguide structure must be sufficiently narrow to decrease radiation loss because a wide spacing can cause to increase insertion loss.

Planar dielectric waveguide filters with cross coupling were developed for 60 GHz band applications. The filters were fabricated using LTCC (Low Temperature Cofired Ceramics) for transceiver module. These filters will be applied to high-speed wireless communication systems.

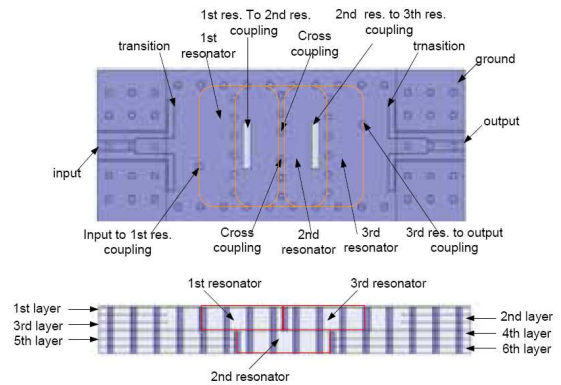


Figure 1: Schematic layout of BPF.

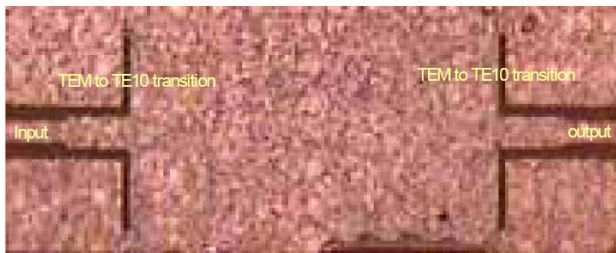


Figure 2: Photograph of a fabricated BPF.

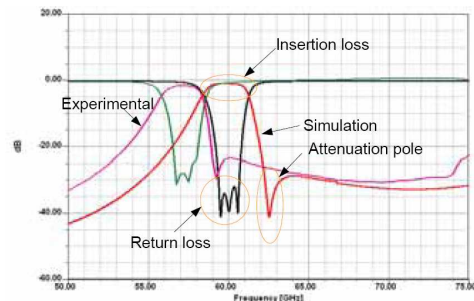


Figure 3: Experimental and simulation results of BPF.